



A model for transient diffusion in bidisperse pore structures

Wei Sun¹ · Sheng-Li Chen¹ · Ming-Ri Xu¹ · Ya-Qian Wei¹ · Ting-Ting Fan¹ · Bao-Li Ma² · Jin-Tao Guo²

Received: 14 January 2019
© The Author(s) 2019

Abstract

A bidisperse model for transient diffusion and adsorption processes in porous materials is presented in this paper. The mathematical model is solved by numerical methods based on finite elements combined with the linear driving force approximation. A criterion based on the model to identify the diffusion controlling mechanism (macropore diffusion, micropore diffusion, or both) is proposed. The effects of different adsorption isotherms (linear, Freundlich, or Langmuir) on the concentration profiles and on curves of fractional uptake versus time are investigated. In addition, the influences of model parameters concerning the pore networks on the fractional uptake are studied as well.

Keywords Transient diffusion · Adsorption · Bidisperse pores · Macropore · Micropore · Linear driving force

List of symbols

C_A	Concentration of the adsorbate A in the pores, mol/m ³
C_{A0}	Concentration of the adsorbate A in the bulk fluid, mol/m ³
$\overline{C_{Ai}}$	Average radial concentration in micropores defined by Eq. (2)
q_A	The amount adsorbed per unit pore surface area on pore walls, mol/m ²
q_m	Monolayer capacity, mol/m ²
q_{A0}	The amount adsorbed on pore walls in equilibrium with C_{A0} , mol/m ²
$\overline{q_{Ai}}$	Average radial concentration on micropore walls defined by Eq. (3)
D	Diffusivity, m ² /s
R_i	Radius of assumed column or nanorod or primary particle, m
L	Length of the membrane or porous slab, m
S	Cross-sectional area of porous membrane or slab in the diffusion direction x , m ²

S_a	Specific surface area of macropores, m ² /kg
S_i	Specific surface area of micropores, m ² /kg
F	Fractional uptake (dimensionless)
n, k_F	Freundlich constant
k_L	Langmuir constant, m ³ /mol
K_L	Langmuir constant (dimensionless)
K	Adsorption parameter (dimensionless)
M_t	Total uptake at given time, mol
M_∞	Total uptake at equilibrium, mol
N	Number of assumed columns in porous materials (dimensionless)
r_i	Spatial coordinate of the cylindrical shell, m
r	Macropore radius, m
d	Inter-macropore distance, m
x	Spatial coordinate through macropore, m
t	Time variable, s
u_1	Concentration in macropores (dimensionless)
u_2	Concentration in micropores (dimensionless)

Greek letters

ε	Porosity based on total volume of porous materials (dimensionless)
ε_i^*	Microporosity based on total volume of assumed columns (dimensionless)
ρ_a	Density of macropore walls, kg/m ³
ρ_i	Skeletal density of porous materials, kg/m ³
α	Diffusion rate parameter (dimensionless)
β	Pore geometry parameter (dimensionless)
γ	Diffusion rate parameter (dimensionless)
τ	Time (dimensionless)

Edited by Xiu-Qin Zhu and Xiu-Qiu Peng

✉ Sheng-Li Chen
slchen@cup.edu.cn

¹ State Key Laboratory of Heavy Oil Processing and Department of Chemical Engineering, China University of Petroleum, Changping, Beijing 102249, People's Republic of China

² Daqing Petrochemical Research Center, CNPC, Daqing 163741, Heilongjiang, China

- κ Defined by Eq. (8) (dimensionless)
 φ Coordinate through macropores (dimensionless)

Subscripts

- a Macropore
 i Micropore

1 Introduction

Porous materials are widely used in chemical industries, such as in heterogeneous catalytic reactions, adsorption, separation and ion exchange. The performance of these chemical engineering processes is sometimes dependent on molecular diffusion inside the pore networks of the porous materials. The pore networks in these porous materials are quite intricate due to the agglomeration of primary particles with micropores. Therefore, two pore subsystems, namely the void between the primary particles and the intrinsic channel inside the primary particles, are connected so that both diffusional resistances affect the molecular mass transport. The porous materials with bidisperse pore structures have attracted the extensive interests of chemical engineers, because in these materials, macropores can be used for intensifying the mass transport and micropores for reaction and adsorption (Bhatia 1997; Lee et al. 1991; Leinekugel-Le-Cocq et al. 2007). The macropores are the voids between the primary particles with the micropores after the tableting or pelleting. Therefore, the use of single diffusivity for simulating of the diffusion inside the bidisperse pore structures may lead to incorrect description of the diffusion process inside such porous materials. Therefore, exact description of the diffusion processes inside the bidisperse pore networks is important for design and optimization of the chemical processes.

For description of the diffusion processes inside bidisperse pore structures, a bidisperse pore model of random pores was proposed by Wakao and Smith (Wakao and Smith 1962), who considered a parallel diffusion mechanism as shown in Fig. 1a: (1) diffusion through the macropores; (2) diffusion through the micropores; (3) diffusion through the macropores and micropores in series. But in this model, steady-state diffusion was assumed. For transient diffusion, Ruckenstein et al. (1971) proposed a globular structure model in which a spherical macroporous pellet was considered as an aggregate of microporous spherical primary particles as shown in Fig. 1b. The adsorbates diffuse into the macropores, and they also are adsorbed on the macropore walls, and this kind of diffusion and adsorption is concurrent in the micropores. This model was widely used (Leitão et al. 1994; Quinta Ferreira

and Rodrigues 1993; Silva and Rodrigues 1996; Taqvi et al. 1997). Another bidisperse pore model of branched micro-macropores was proposed by Turner (Turner 1958), who considered the shape of macropores being a cylinder branched with several cylindrical micropores as shown in Fig. 1c. Because of its simplicity, Turner's model was used extensively to describe the diffusion and reaction or adsorption in bidisperse pores (Mann and Thomson 1987; Petersen 1991; Tartarelli et al. 1970). Based on Turner's model, Silva and Rodrigues (Silva and Rodrigues 1999) made an extension of Ruckenstein's work to non-linear adsorption equilibrium with negligible macropore adsorption. However, in the globular structure model and branched micro-macropore model, Ruckenstein et al. and Turner all considered that the adsorbates diffused into the macropores preferentially, and then diffused into micropores. But actually, for transient diffusion, besides the diffusion paths in the globular structure model by Ruckenstein et al. and the branched micro-macropore model by Turner, there is another parallel diffusion path through micropores (denoted by the blue arrow shown in Fig. 2c) as presented in the random pore model.

In this paper, a model is proposed for transient diffusion and adsorption in porous materials with bidisperse pore structures. In this model, the diffusion path is divided into two parallel paths (as shown in Fig. 2c): (1) molecules diffuse into macropores, and are adsorbed on the macropore walls, then diffuse into micropores and are adsorbed on the micropore walls (only this path was involved in Ruckenstein and Turner's models); (2) molecules diffuse through micropores and then are adsorbed on the micropore walls. Three types of adsorption equilibrium isotherms (linear, Freundlich, Langmuir) are considered in this work. The effects of the nature of the adsorption equilibrium isotherm on the concentration profiles in bidisperse pores and on curves of fractional uptake versus time are investigated. The effects of model parameters on the curves of fractional uptake are studied as well and a criterion to identify the controlling mechanisms which reflect the competing effects of macropore and micropore diffusion is proposed.

2 Mathematical models

2.1 Basic equations

In chemical engineering, there is a type of porous materials with a honeycomb structure, such as the porous aluminum membrane of anodic aluminum oxide (AAO) (Evans et al. 2000; Lee and Park 2014; Masuda and Fukuda 1995; Xu et al.

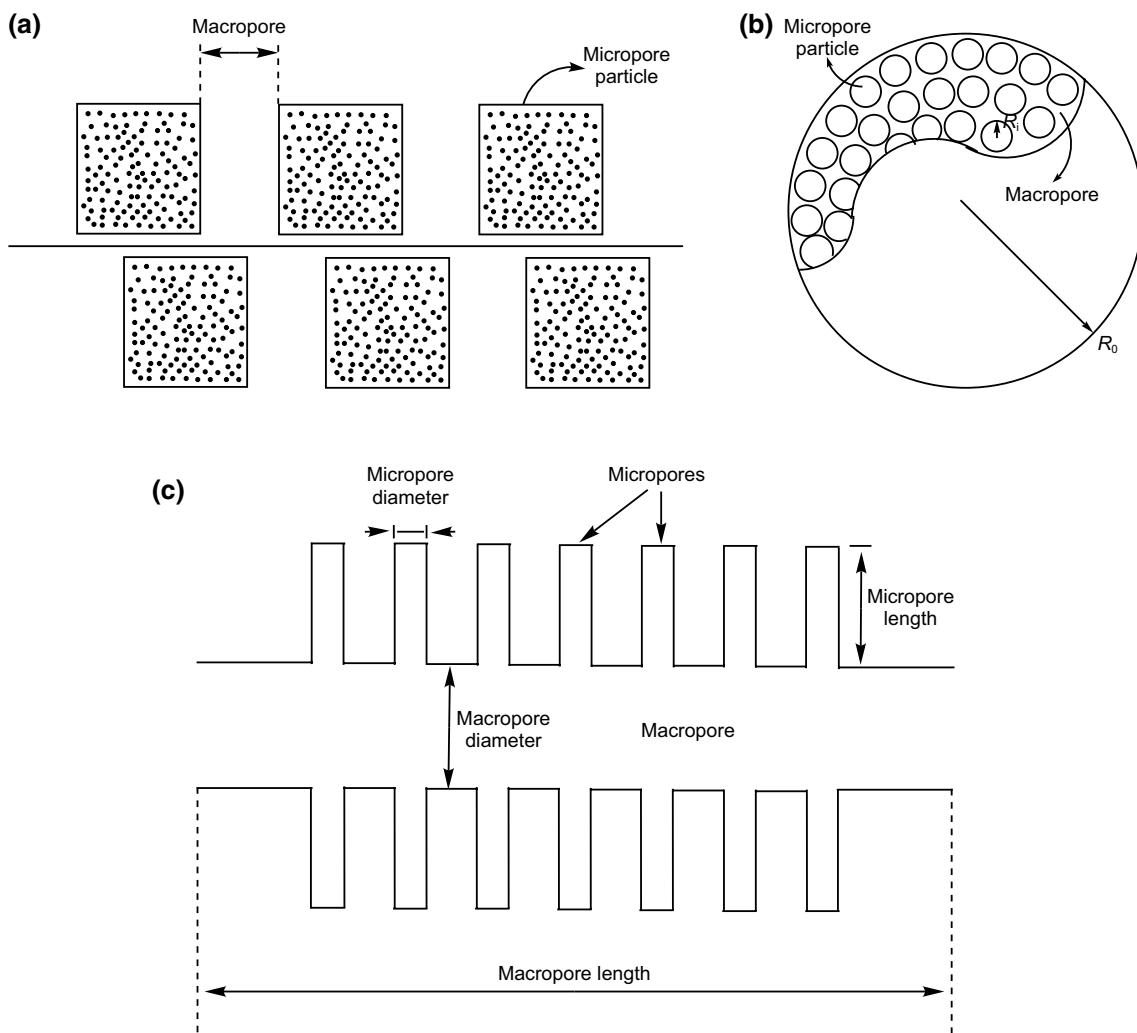


Fig. 1 Schematic representation of the **a** random pore model, **b** globular structure model and **c** branched micro-macropore model

2000), and some well-known zeolites of SBA-15 (Chu et al. 2014; Do et al. 2004; Zhao et al. 1998; Zhu et al. 2012) and MCM-41 (Muñoz et al. 2003; Selvam et al. 2001; Vallet-Regi et al. 2001; Zhao and Lu 1998). Because of their unique pore structures, these porous materials are widely used in separation and adsorption (Vinu et al. 2004; Nguyen et al. 2008; Shi et al. 2008). These porous materials have some orderly arranged pores, for example, Fig. 2a shows the pore structure of an AAO membrane. Initially, such membrane or slab is empty of adsorbate at time zero. Then a step change in the concentration of adsorbate A at the external surface of such membrane or slab occurs, and the diffusion of the adsorbate A into the membrane or slab starts. In this work, the pore geometry was treated mathematically for a convenient description of the diffusion processes: considering a basic pore unit as shown in Fig. 2b, a column is assumed, of which the cross-sectional area perpendicular to the macropore direction is

equal to the micropore area. The equivalent radius R_i of the assumed column can be calculated by the following equation (see “Appendix A”):

$$R_i = \sqrt{\frac{\sqrt{3}}{4\pi}d^2 - \frac{1}{2}r^2}$$

where d is the inter-macropore distance, m; r is the macropore radius, m. The length L of the column is the membrane or slab thickness, m. Under this assumption, the porous membrane or slab is viewed as an assembly of numerous uniform microporous columns shown in Fig. 2c. Macropores become the voids between the assumed columns. The diffusion of adsorbates into these pores is described as follows.

There are two parallel diffusion paths through an arbitrary cross-sectional area (shown in the red color in Fig. 2c),

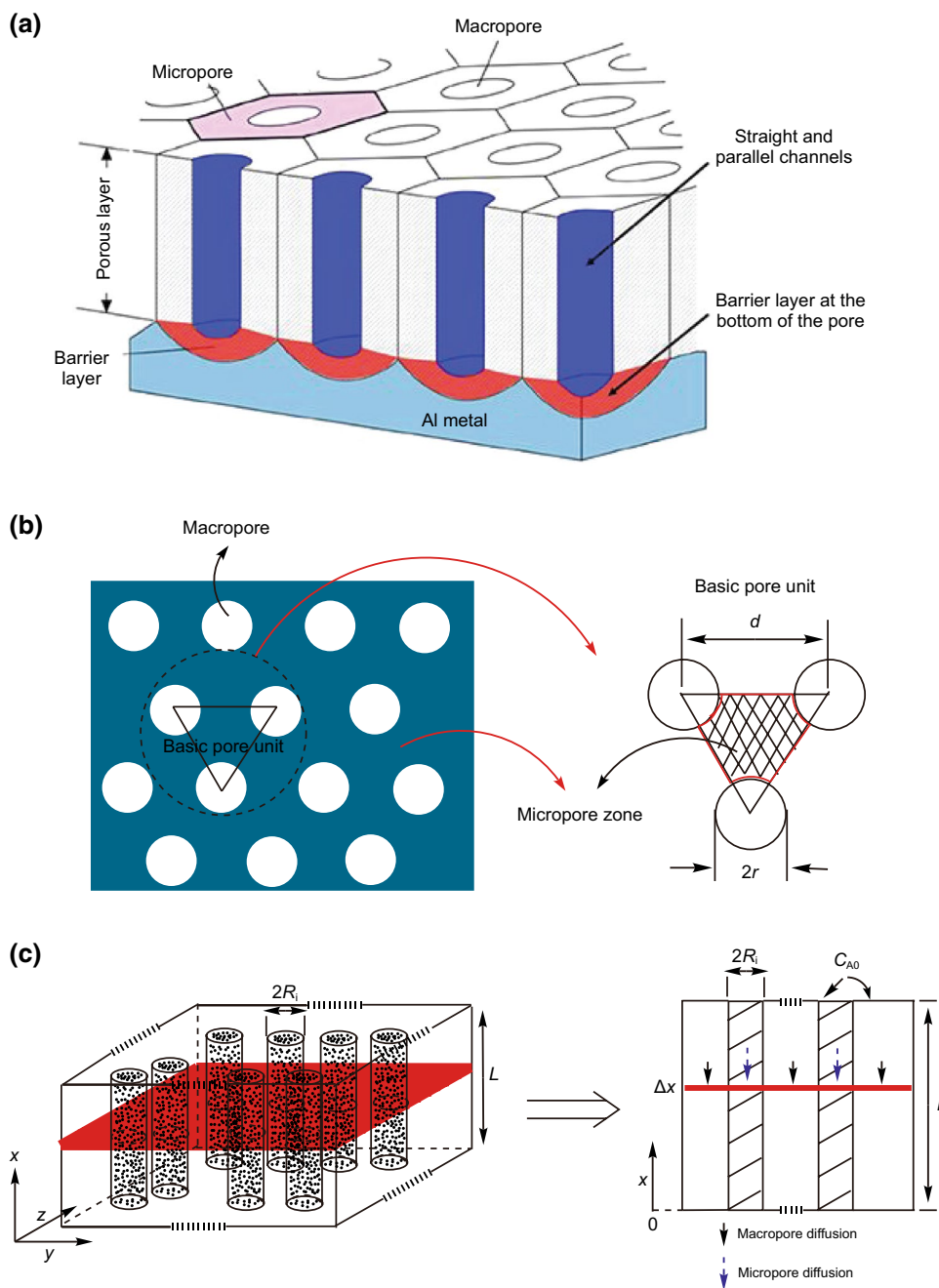


Fig. 2 Schematic representation of the **a** pore structure of the porous membrane of anodic aluminum oxide (AAO), **b** basic pore unit of porous materials (membrane or slab) with a honeycomb bidisperse pore structure and **c** diffusion of molecules into assumed columns in a membrane or slab with bidisperse pores

which is perpendicular to the x direction in the membrane or slab, and they are macropore diffusion and micropore diffusion as shown in Fig. 2c:

(1) The adsorbates diffuse into the macropores and are also adsorbed on the macropore walls, meanwhile the adsorbates diffuse into micropores and are adsorbed on micropore walls.

(2) The adsorbates diffuse into the micropores and are also adsorbed on the micropore walls.

The mass balance for an arbitrary cross-sectional area (red part in Fig. 2c) at any time is

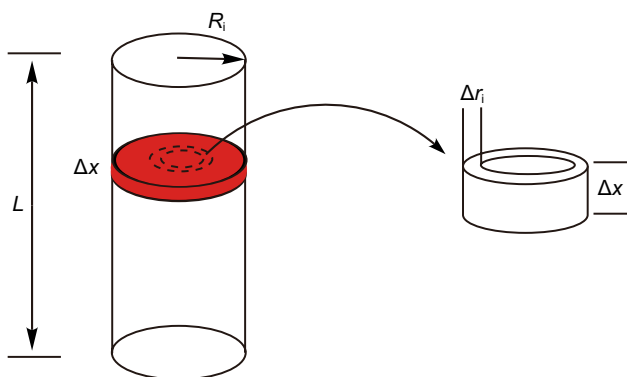


Fig. 3 Schematic diagram of a single assumed column

$$\begin{aligned} \epsilon_a \frac{\partial}{\partial x} \left[D_a \frac{\partial C_{Aa}}{\partial x} \right] + \epsilon_i \frac{\partial}{\partial x} \left[D_i \frac{\partial \overline{C_{Ai}}}{\partial x} \right] &= \epsilon_a \frac{\partial C_{Aa}}{\partial t} + (1 - \epsilon_a) \rho_a S_a \frac{\partial q_{Aa}}{\partial t} \\ + \epsilon_i \frac{\partial \overline{C_{Ai}}}{\partial t} + (1 - \epsilon_a - \epsilon_i) \rho_s S_i \frac{\partial \overline{q_{Ai}}}{\partial t} \end{aligned} \quad (1)$$

where

$$\overline{C_{Ai}} = \frac{1}{\pi R_i^2} \int_0^{R_i} C_{Ai} 2\pi r_i dr_i = \frac{2}{R_i^2} \int_0^{R_i} C_{Ai} r_i dr_i \quad (2)$$

$$\overline{q_{Ai}} = \frac{1}{\pi R_i^2} \int_0^{R_i} q_{Ai} 2\pi r_i dr_i = \frac{2}{R_i^2} \int_0^{R_i} q_{Ai} r_i dr_i \quad (3)$$

$\overline{C_{Ai}}$ and $\overline{q_{Ai}}$ are, respectively, the average concentration in micropores and the average amount adsorbed on micropore walls of the assumed column in a radial direction (shown in Fig. 3). D_a and D_i are the diffusivities in macro- and micropores, respectively, m^2/s ; C_{Aa} and C_{Ai} represent the concentration of adsorbate A in the macro- and micropores, respectively, mol/m^3 ; q_{Aa} and q_{Ai} represent the amount of adsorbate A adsorbed on macro- and micropore walls, respectively, based on per unit pore surface area, mol/m^2 ; x is the spatial coordinate of the cross-sectional area, m ; r_i is the spatial coordinate of the cylindrical shell shown in Fig. 3, m ; ϵ_a and ϵ_i represent the macro- and microporosity, respectively, based on the total volume of the bidisperse porous materials; ρ_a is the density of macroporous walls in the bidisperse porous materials and ρ_s is the skeletal density of the bidisperse porous materials, kg/m^3 ; S_a and S_i represent the specific surface area of macro- and micropore, respectively, m^2/kg ; t is the time variable, s .

The first and second terms of Eq. (1) represent the variation of diffusion flux in the macro- and micropores, respectively. The third and fourth terms are related to the

accumulation of adsorbates in macropore volumes and on macropore walls, respectively. The last two terms are related to the accumulation of adsorbates in micropore volumes and on micropore walls, respectively. When the concentration of adsorbate A in the solution on the outside surface of the porous membrane or slab is constant and equals to that of the bulk liquid, the initial and boundary conditions are

$$\begin{cases} C_{Aa}(0, x) = 0; & \overline{C_{Ai}}(0, x) = 0 \\ \frac{\partial C_{Aa}}{\partial x}(t, 0) = 0; & \frac{\partial \overline{C_{Ai}}}{\partial x}(t, 0) = 0 \\ C_{Aa}(t, L) = C_{A0}; & \overline{C_{Ai}}(t, L) = C_{A0} \end{cases} \quad (4)$$

The amount of adsorbate A adsorbed on the pore walls can be related to the concentration of adsorbate A in pore volumes by the adsorption equilibrium isotherm (Ruckenstein et al. 1971; Silva and Rodrigues 1999). Three adsorption isotherms are considered in this work:

Linear isotherm $q_A = \left(\frac{q_{A0}}{C_{A0}} \right) \cdot C_A \quad (5a)$

Freundlich isotherm $q_A = k_F \cdot (C_A)^n \quad (5b)$

Langmuir isotherm $q_A = q_m \frac{k_L C_A}{1 + k_L C_A} \quad (5c)$

where q_A is the amount adsorbed on pore walls per unit pore surface area, mol/m^2 ; C_A is the concentration of adsorbate A in pore volumes, mol/m^3 ; q_{A0} is the amount adsorbed on pore walls at concentration C_{A0} ; k_F and n are the Freundlich constants, the unit of k_F is m^{2n-2}/mol^{n-1} and n is a dimensionless constant; k_L is the Langmuir constant, m^3/mol ; q_m is the monolayer adsorption capacity, mol/m^2 .

The mass balance for an arbitrary cylindrical shell with height of Δx and thickness of Δr_i in a single assumed column (shown in Fig. 3) is

$$D_i \frac{\epsilon_i^* \kappa}{r_i} \frac{\partial}{\partial r_i} \left[r_i \frac{\partial C_{Ai}}{\partial r_i} \right] + D_i \epsilon_i^* \frac{\partial}{\partial x} \left[\frac{\partial C_{Ai}}{\partial x} \right] = \epsilon_i^* \frac{\partial C_{Ai}}{\partial t} + (1 - \epsilon_i^*) \rho_s S_i \frac{\partial \overline{q_{Ai}}}{\partial t} \quad (6)$$

where ϵ_i^* is the microporosity based on the microporous columns and it is related to the ϵ_i and ϵ_a based on the total volume of the porous materials by Eq. (7)

$$\frac{\epsilon_i^*}{1 - \epsilon_i^*} = \frac{\epsilon_i}{1 - \epsilon_a - \epsilon_i} \quad (7)$$

κ is the ratio of accessible area of adsorbates diffusing from macropore to micropore to the total lateral area of the

arbitrary cylindrical shell and the κ is expressed by Eq. (8) (shown in “Appendix A”)

$$\kappa = \begin{cases} 1 & \text{Nanorod structure} \\ \frac{\pi}{\sqrt{3\pi m^2 - 2\pi^2}} (m = \frac{d}{r} \geq 2) & \text{Honeycomb structure} \end{cases} \quad (8)$$

$\kappa = 1$ is for the bidisperse porous materials composed of a porous nanorod array (Lu et al. 2004). Based on Eq. (7), Eq. (6) can be transformed into Eq. (9):

$$D_i \frac{\varepsilon_i \kappa}{r_i} \frac{\partial}{\partial r_i} \left[r_i \frac{\partial C_{Ai}}{\partial r_i} \right] + D_i \varepsilon_i \frac{\partial}{\partial x} \left[\frac{\partial C_{Ai}}{\partial x} \right] = \varepsilon_i \frac{\partial C_{Ai}}{\partial t} + (1 - \varepsilon_a - \varepsilon_i) \rho_s S_i \frac{\partial q_{Ai}}{\partial t} \quad (9)$$

The first and second terms of Eq. (9) represents the variation of diffusion flux in the micropore in the direction of the spatial coordinate r_i and x , respectively. The third and fourth terms are related to the accumulation in micropore volumes and on micropore walls, respectively. The initial and boundary conditions are:

$$\begin{cases} C_{Ai}(0, x, r_i) = 0 \\ \frac{\partial C_{Ai}}{\partial x}(t, 0, r_i) = 0; \quad \frac{\partial C_{Ai}}{\partial r_i}(t, x, 0) = 0 \\ C_{Ai}(t, L, r_i) = C_{A0}; \quad C_{Ai}(t, x, R_i) = C_{Aa} \end{cases} \quad (10)$$

Due to the complexity of the mathematical model, analytic solutions are difficult to obtain. For solving the partial differential Eqs. (1) and (9), a numerical solution is proposed in this work. Complete numerical solutions for Eq. (9) need spatial discretization of both the r_i and x as well as the time t discretization. Substantial saving in computing time can be achieved by eliminating r_i spatial discretization by the method of the linear driving force (LDF) approximation first suggested by Glueckauf and Coates (Glueckauf and Coates 1947). With the assumption of a parabolic concentration profile in the radial direction r_i (Liaw et al. 1979), the partial differential Eqs. (1) and (9) can be transformed into Eqs. (11) and (12), respectively (the explicit transforming steps are shown in “Appendix B”):

$$\varepsilon_a \frac{\partial C_{Aa}}{\partial t} + (1 - \varepsilon_a) \rho_a S_a \frac{\partial q_{Aa}}{\partial t} = \varepsilon_a D_a \frac{\partial}{\partial x} \left[\frac{\partial C_{Aa}}{\partial x} \right] - \frac{8\varepsilon_i \kappa D_i}{R_i^2} (C_{Aa} - \overline{C_{Ai}}) \quad (11)$$

$$\varepsilon_i \frac{\partial \overline{C_{Ai}}}{\partial t} + (1 - \varepsilon_a - \varepsilon_i) \rho_s S_i \frac{\partial \overline{q_{Ai}}}{\partial t} = \varepsilon_i D_i \frac{\partial}{\partial x} \left[\frac{\partial \overline{C_{Ai}}}{\partial x} \right] + \frac{8\varepsilon_i \kappa D_i}{R_i^2} (C_{Aa} - \overline{C_{Ai}}) \quad (12)$$

where

$$\frac{\partial q_{Aa}}{\partial t} = \frac{\partial q_{Aa}}{\partial C_{Aa}} \cdot \frac{\partial C_{Aa}}{\partial t} \quad (13)$$

$$\frac{\partial \overline{q_{Ai}}}{\partial t} = \frac{\partial \overline{q_{Ai}}}{\partial \overline{C_{Ai}}} \cdot \frac{\partial \overline{C_{Ai}}}{\partial t} \quad (14)$$

Introducing the following dimensionless variables:

For the fluid phase concentration in macro- and micropore volume, respectively

$$u_1 = \frac{C_{Aa}}{C_{A0}}, \quad u_2 = \frac{\overline{C_{Ai}}}{C_{A0}}$$

For the spatial coordinate

$$\varphi = \frac{x}{L}$$

For the time coordinate

$$\tau = \frac{D_a}{L^2} t$$

and parameters

$$\alpha = \frac{D_i}{R_i^2} \frac{L^2}{D_a}; \quad \beta = \frac{\varepsilon_i}{\varepsilon_a}; \quad \gamma = \frac{D_i}{D_a}; \quad K_a = \frac{(1 - \varepsilon_a) \rho_a S_a \frac{q_{A0}}{C_{A0}}}{\varepsilon_a};$$

$$K_i = \frac{(1 - \varepsilon_a - \varepsilon_i) \rho_s S_i \frac{q_{A0}}{C_{A0}}}{\varepsilon_i}; \quad K_L = k_L C_{A0}$$

The partial differential Eqs. (11) and (12) for mass balance, respectively, become:

For the linear isotherm

$$[1 + K_a] \frac{\partial u_1}{\partial \tau} = \frac{\partial^2 u_1}{\partial \varphi^2} - 8\alpha\beta\kappa(u_1 - u_2) \quad (15a)$$

$$[1 + K_i] \frac{\partial u_2}{\partial \tau} = \gamma \frac{\partial^2 u_2}{\partial \varphi^2} + 8\alpha\kappa(u_1 - u_2) \quad (15b)$$

For the Freundlich isotherm

$$[1 + K_a n \cdot (u_1)^{n-1}] \frac{\partial u_1}{\partial \tau} = \frac{\partial^2 u_1}{\partial \varphi^2} - 8\alpha\beta\kappa(u_1 - u_2) \quad (16a)$$

$$[1 + K_i n \cdot (u_2)^{n-1}] \frac{\partial u_2}{\partial \tau} = \gamma \frac{\partial^2 u_2}{\partial \varphi^2} + 8\alpha\kappa(u_1 - u_2) \quad (16b)$$

For the Langmuir isotherm

$$\left[1 + K_a \frac{1 + K_L}{(1 + K_L u_1)^2} \right] \frac{\partial u_1}{\partial \tau} = \frac{\partial^2 u_1}{\partial \varphi^2} - 8\alpha\beta\kappa(u_1 - u_2) \quad (17a)$$

$$\left[1 + K_i \frac{1 + K_L}{(1 + K_L u_2)^2} \right] \frac{\partial u_2}{\partial \tau} = \gamma \frac{\partial^2 u_2}{\partial \varphi^2} + 8\alpha\kappa(u_1 - u_2) \quad (17b)$$

The initial and boundary conditions of the above partial differential equations for three types of isotherms are:

$$\begin{cases} u_1(0, \varphi) = 0; & u_2(0, \varphi) = 0 \\ \frac{\partial u_1}{\partial \varphi}(\tau, 0) = 0; & \frac{\partial u_2}{\partial \varphi}(\tau, 0) = 0 \\ u_1(\tau, 1) = 1; & u_2(\tau, 1) = 1 \end{cases}$$

At any time t , the total uptake M_t is evaluated by determining the adsorbate in the porous materials. The total uptake can be divided into two parts. One is the amount of adsorbate in the macropores:

$$M_{ta} = \int_0^L C_{Aa} \varepsilon_a S dx + \int_0^L q_{Aa} (1 - \varepsilon_a) \rho_a S_a S dx \quad (18)$$

where S is the cross-sectional area of porous membrane or slab perpendicular to the diffusion direction x , m^2 . The other is the amount of adsorbate located in the micropores:

$$M_{ti} = N \int_0^L \int_0^{R_i} [C_{Ai} \varepsilon_i^* + q_{Ai} (1 - \varepsilon_i^*) \rho_s S_i] 2\pi r_i dr_i dx \quad (19)$$

where N is the number of the columns in the porous materials and can be expressed by following Eq. (20):

$$N = \frac{S(1 - \varepsilon_a)}{\pi R_i^2} \quad (20)$$

The total uptake M_t at any time t is:

$$M_t = M_{ta} + M_{ti} \quad (21)$$

The total uptake at equilibrium, M_∞ , is:

$$M_\infty = SL[\varepsilon_a C_{A0} + (1 - \varepsilon_a) \rho_a S_a q_{A0}] + SL[\varepsilon_i C_{A0} + (1 - \varepsilon_a - \varepsilon_i) \rho_s S_i q_{A0}] \quad (22)$$

The fractional uptake F is defined as:

$$F = \frac{M_t}{M_\infty} \quad (23)$$

For the linear isotherm

$$F = \frac{(1 + K_a) \int_0^1 u_1 d\varphi + \beta(1 + K_i) \int_0^1 u_2 d\varphi}{[1 + K_a] + \beta[1 + K_i]} \quad (24)$$

For the Freundlich isotherm

$$F = \frac{\int_0^1 [u_1 + K_a(u_1)^n] d\varphi + \beta \int_0^1 [u_2 + K_i(u_2)^n] d\varphi}{[1 + K_a] + \beta[1 + K_i]} \quad (25)$$

For the Langmuir isotherm

$$F = \frac{\int_0^1 \left[1 + K_a \frac{(1+K_L)}{1+K_L u_1} \right] u_1 d\varphi + \beta \int_0^1 \left[1 + K_i \frac{(1+K_L)}{1+K_L u_2} \right] u_2 d\varphi}{[1 + K_a] + \beta[1 + K_i]} \quad (26)$$

2.2 Numerical solutions to the mathematical models

The numerical solutions to the pair of coupled partial differential Eqs. (15)–(17) (15a, b; 16a, b; 17a, b) are obtained by using the pdepe solver package of MATLAB (version 2017a). The partial differential equations for Freundlich isotherms (16a, b; $n < 1$) and Langmuir isotherms (17a, b) are singular at the initial conditions, $\tau = 0$. The initial conditions for Freundlich ($n < 1$) and Langmuir isotherms are therefore replaced by small values (Arocha et al. 1996):

$$\tau = 0, \quad 0 \leq \varphi \leq 1, \quad u_1 = u_2 = 1 \times 10^{-10} \quad (27)$$

For the linear isotherm and the Freundlich isotherm ($n > 1$), this approximation is not needed because the equations are regular at initial conditions.

3 Results and discussion

The parameter α can be written as (Ruckenstein et al. 1971):

$$\alpha = \frac{D_i L^2}{R_i^2 D_a} = \frac{\frac{D_i}{R_i^2}}{\frac{D_a}{L^2}} = \frac{t_m}{t_i}$$

where t_m gives the order of magnitude of time required for penetration of adsorbate through the macropores by diffusion. t_i is the time required for penetration of adsorbate through the micropores by diffusion in the r_i direction. Therefore, α represents the ratio of time scale of diffusion processes occurring in macropores and in micropores (in the r_i direction). The parameter β is the ratio of micro- and macroporosity, which gives the information about the capacity of adsorbate in micro- and macropores. The parameter γ is the ratio of diffusivity in micropores to that in macropores. The parameter α/γ gives the ratio of diffusion length

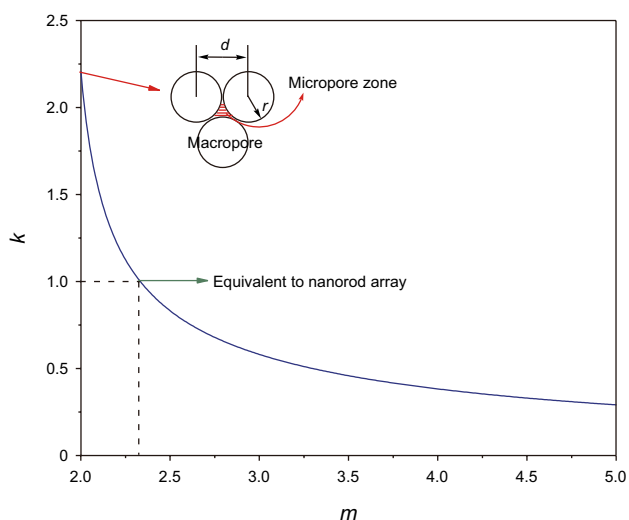


Fig. 4 The profile of parameter κ versus m

required for diffusion of adsorbate through the macropores and micropores. The parameter α/γ is expressed as:

$$\frac{\alpha}{\gamma} = \frac{L^2}{R_i^2}$$

The parameters K_a and K_i give information concerning the ratio of capacity of adsorbate on pore walls and in pore volumes, for macro- and micropores, respectively. Parameters n and K_L express the nonlinearity of the isotherms, respectively, for Freundlich and Langmuir isotherms. Parameter κ concerns the accessible area of adsorbates diffusing from macropore to micropore. For porous materials composed of porous nanorods, $\kappa = 1$; for porous materials with a honeycomb structure, κ depends on the ratio (m) of inter-macropore distance and macropore size as shown in Fig. 4.

3.1 A criterion to determine the diffusion controlling mechanism

For small values of $\alpha < 0.001$, the time required for adsorbates diffusing through the micropores in r_i direction is much longer than that required for diffusion through the macropores ($t_i \gg t_m$), indicating the diffusion in macropores is much faster than that in micropores. Under this situation, when the uptake process of adsorbates in macropores is at equilibrium, no adsorbates diffuse into the micropores (see Figs. 5, 6). This means that mass transfer in the porous materials is limited by the micropore diffusion.

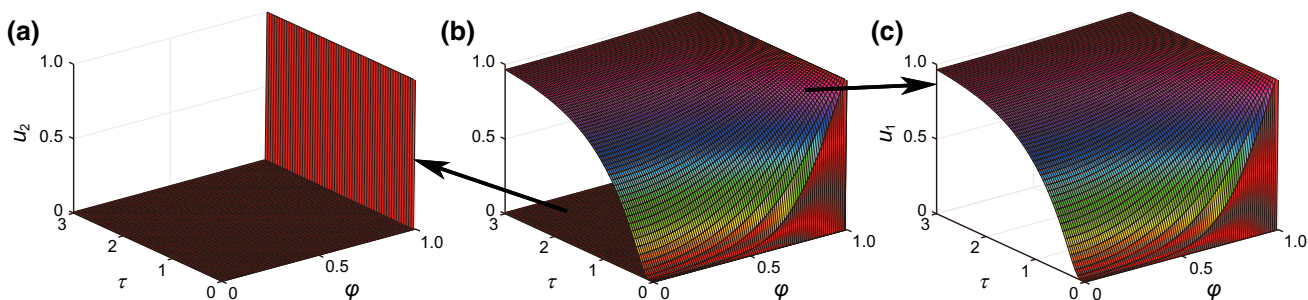


Fig. 5 The dimensionless concentration profiles for a linear isotherm with $\alpha=0.001$, $\beta=1$, $\alpha/\gamma=20,000$, $K_a=1$, $K_i=1$, $\kappa=1$: micropore diffusion control. **a** Dimensionless micropore fluid concentration u_2 versus τ and φ . **b** Dimensionless fluid concentration profiles u_1 and u_2 versus τ and φ (combined figure). **c** Dimensionless macropore fluid concentration u_1 versus τ and φ

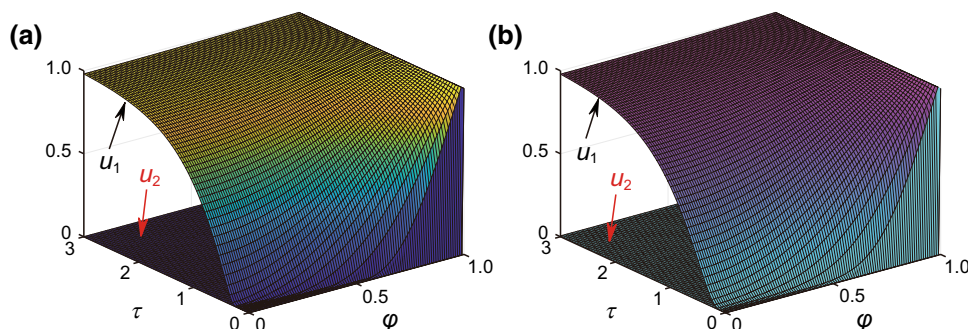


Fig. 6 The dimensionless concentration profiles u_1 (in macropores) and u_2 (in micropores) versus τ and φ for two types of isotherms with $\alpha=0.001$, $\beta=1$, $\alpha/\gamma=20,000$, $K_a=1$, $K_i=1$, $\kappa=1$: micropore diffusion control. **a** Freundlich isotherm, $n=0.5$. **b** Langmuir isotherm, $K_L=1$

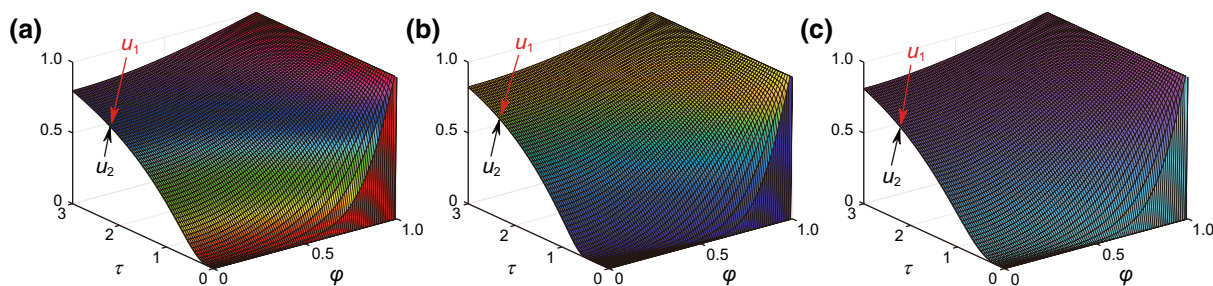


Fig. 7 The dimensionless concentration profiles u_1 (in macropores) and u_2 (in micropores) versus τ and φ for three types of isotherms with $\alpha=10$, $\beta=1$, $\alpha\gamma=20,000$, $K_a=1$, $K_i=1$, $\kappa=1$: macropore diffusion control. **a** Linear isotherm. **b** Freundlich isotherm, $n=0.5$. **c** Langmuir isotherm, $K_L=1$

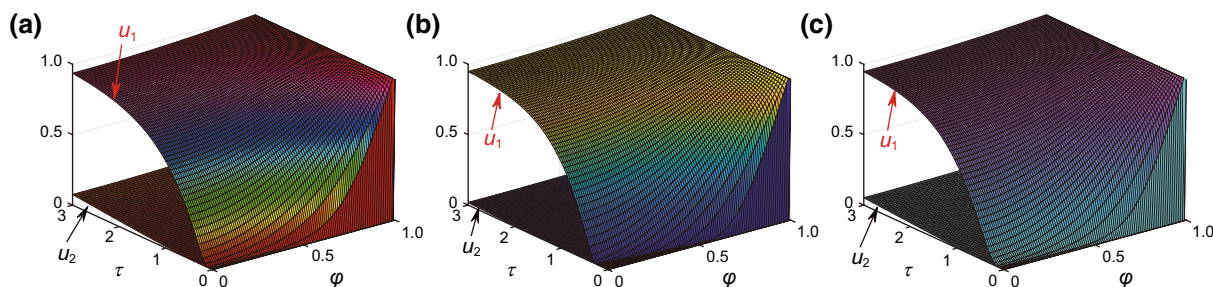


Fig. 8 The dimensionless concentration profiles u_1 (in macropores) and u_2 (in micropores) versus τ and φ for three types of isotherms with $\alpha=0.01$, $\beta=1$, $\alpha\gamma=20,000$, $K_a=1$, $K_i=1$, $\kappa=1$: macropore and micropore diffusion control. **a** Linear isotherm. **b** Freundlich isotherm, $n=0.5$. **c** Langmuir isotherm, $K_L=1$

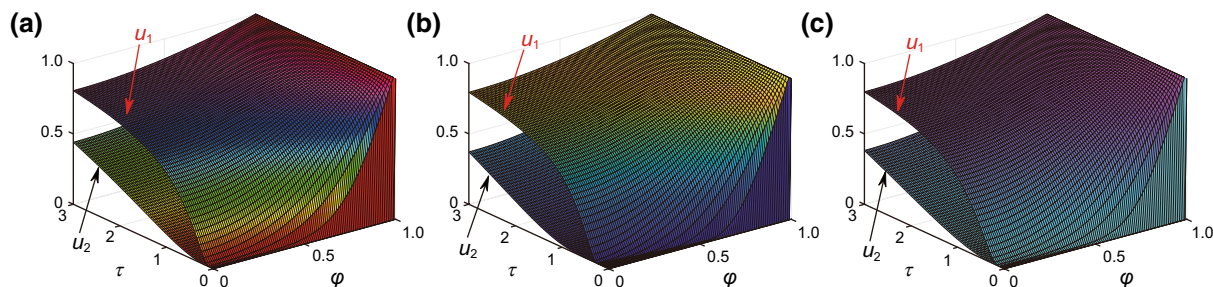


Fig. 9 The dimensionless concentration profiles u_1 (in macropores) and u_2 (in micropores) versus τ and φ for three types of isotherms with $\alpha=0.1$, $\beta=1$, $\alpha\gamma=20,000$, $K_a=1$, $K_i=1$, $\kappa=1$: macropore and micropore diffusion control. **a** Linear isotherm. **b** Freundlich isotherm, $n=0.5$. **c** Langmuir isotherm, $K_L=1$

A second limiting case is for the large value of α . When the value of α is sufficiently large ($\alpha > 10$), the diffusion of adsorbates in micropores is faster than that in macropores. As shown in Fig. 7, the 3D (three-dimensional) surface plots of dimensionless concentration u_1 (in macropores) and u_2 (in micropores) are almost overlapped, which means that the diffusion processes of adsorbates into macropores and into micropores can be considered as a synchronous process. Consequently, the whole mass transfer in the porous materials is limited by the macropore diffusion.

For the intermediate value of $0.001 < \alpha < 10$, concentration gradients exist both in macro- and micropores and also exist between macro- and micropores (see Figs. 8, 9, 10). Under this situation, the whole mass transfer in the porous materials is controlled by both macropore and micropore diffusion.

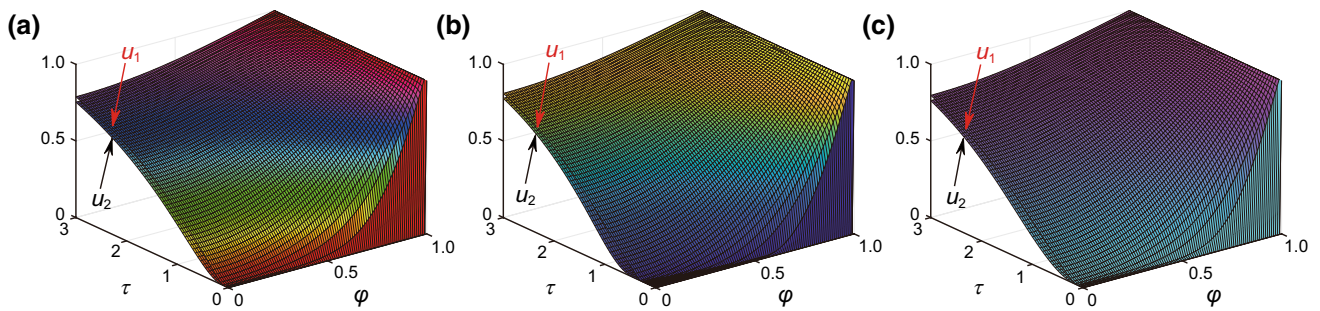


Fig. 10 The dimensionless concentration profiles u_1 (in macropores) and u_2 (in micropores) versus τ and φ for three types of isotherms with $\alpha=1, \beta=1, \alpha/\gamma=20,000, K_a=1, K_i=1, \kappa=1$: macropore and micropore diffusion control. **a** Linear isotherm. **b** Freundlich isotherm, $n=0.5$. **c** Langmuir isotherm, $K_L=1$

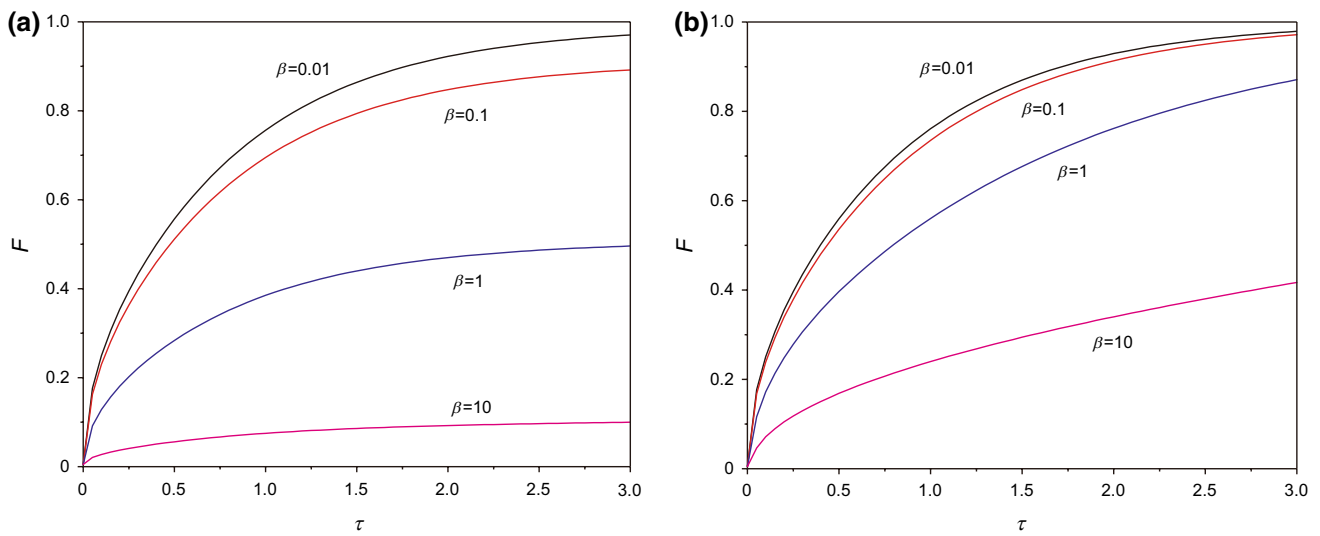


Fig. 11 The fractional uptake F profiles versus τ for linear isotherm with $\alpha/\gamma=20,000, K_a=1, K_i=1, \kappa=1$. **a** $\alpha=0.001$, micropore diffusion control. **b** $\alpha=10$, macropore diffusion control

3.2 Effects of model parameters on the fractional uptake

Figure 11 shows the fractional uptake F at the limiting cases of micropore diffusion control ($\alpha=0.001$, Fig. 11a) and macropore diffusion control ($\alpha=10$, Fig. 11b) with different values of β . It can be seen that for a small value of $\alpha=0.001$, the profiles of fractional uptake have a plateau at large values of β , indicating that the uptake processes can be divided into two stages. The first stage is attributed to the very fast uptake in macropores, and the second stage (plateau) mainly is attributed to the much slower uptake occurring in micropores. But for large values of $\alpha=10$, the profiles of fractional uptake have no plateau appearing due to the comparable diffusion rates in micro- and macropores.

Figure 12 shows the fractional uptake F at the intermediate values of $\alpha=0.01, 0.1, 1$. It can be seen that for a fixed α , the rate of approaching equilibrium increases with decreasing β , indicating that the more macropores exist, the faster the uptake rate is. Similarly, for fixed β , the fractional uptake increases with increasing α , reflecting an increase in the diffusion rate in micropores which contributes to the enhancement of the mass transport in porous materials.

The effect of parameter α/γ on the fractional uptake is shown in Fig. 13. It can be found that at a large value of β (high microporosity), the fractional uptake decreases with increasing α/γ , because for a fixed α , increasing α/γ reflects a decreasing diffusion rate in micropores. For a small value of $\beta=0.1$, the curves of fractional uptake at different

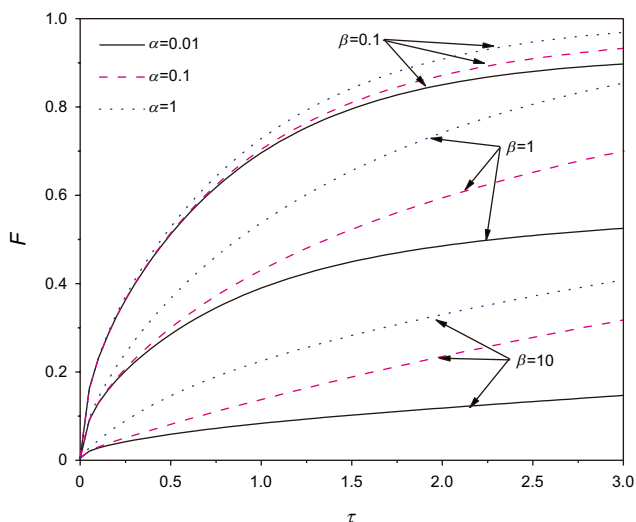


Fig. 12 The fractional uptake F profiles versus τ for a linear isotherm at intermediate values of $\alpha=0.01, 0.1, 1$ with $\alpha/\gamma=20,000, K_a=1, K_i=1, \kappa=1$: macropore and micropore diffusion control

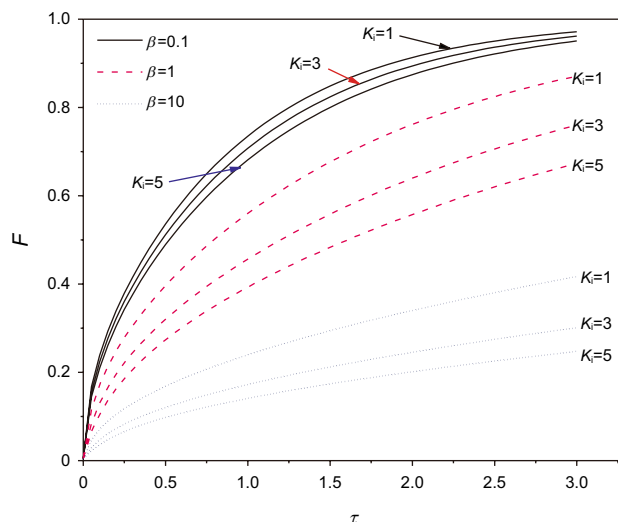


Fig. 14 The effect of parameter K_i on fractional uptake F for a linear isotherm with $\alpha=10, \alpha/\gamma=20,000, K_a=1, \kappa=1$

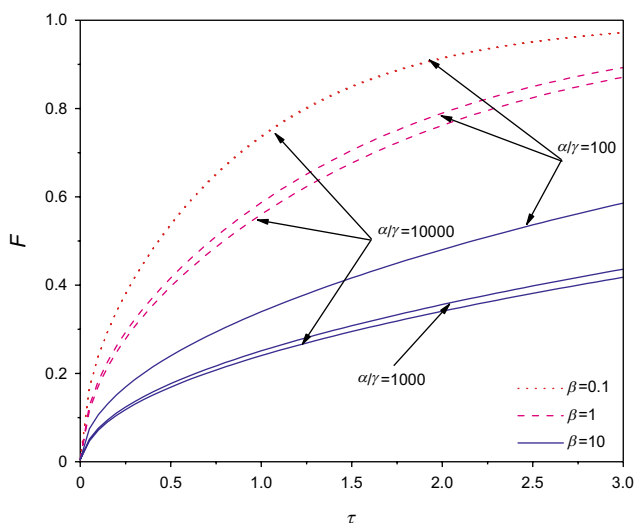


Fig. 13 The effect of parameter α/γ on fractional uptake F for a linear isotherm with $\alpha=10, K_a=1, K_i=1, \kappa=1$

values of α/γ are overlapped. It also can be seen that for a fixed value of $\beta=10$, the curve of fractional uptake at value of $\alpha/\gamma=1000$ is close to being overlapped with the curve of fractional uptake at value of $\alpha/\gamma=10,000$, which indicates that for large lumps of porous material, the effect of parameter α/γ on the fractional uptake can be ignored, but it needs to be considered for a thick membrane or film porous materials.

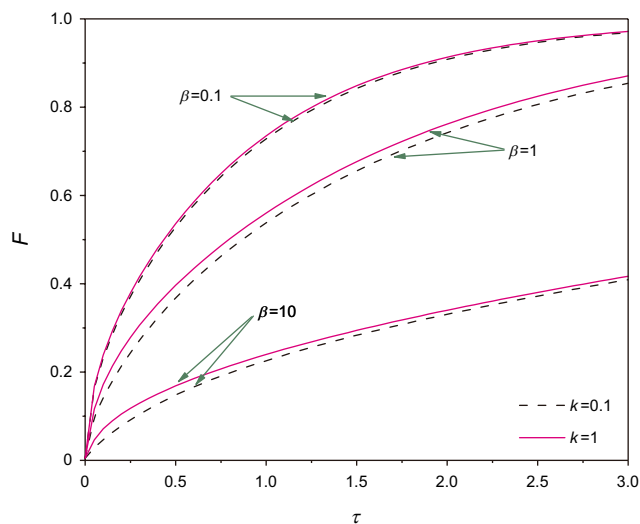


Fig. 15 The effect of parameter κ on fractional uptake F for a linear isotherm with $\alpha=10, \alpha/\gamma=20,000, K_a=1, K_i=1$

Actually for the porous materials used in industry, the specific surface area of the wall of macropores is much lower than that of micropores. Therefore, the value of K_a is much lower than that of K_i ($K_a \ll K_i$). The effect of parameter K_a on the fractional uptake can be ignored in comparison with K_i . Figure 14 shows the effect of parameter K_i on the fractional uptake for a linear isotherm. It can be seen that the fractional uptake decreases with increasing K_i .

The effect of parameter κ on the fractional uptake can be seen in Fig. 15. It is found that the fractional uptake

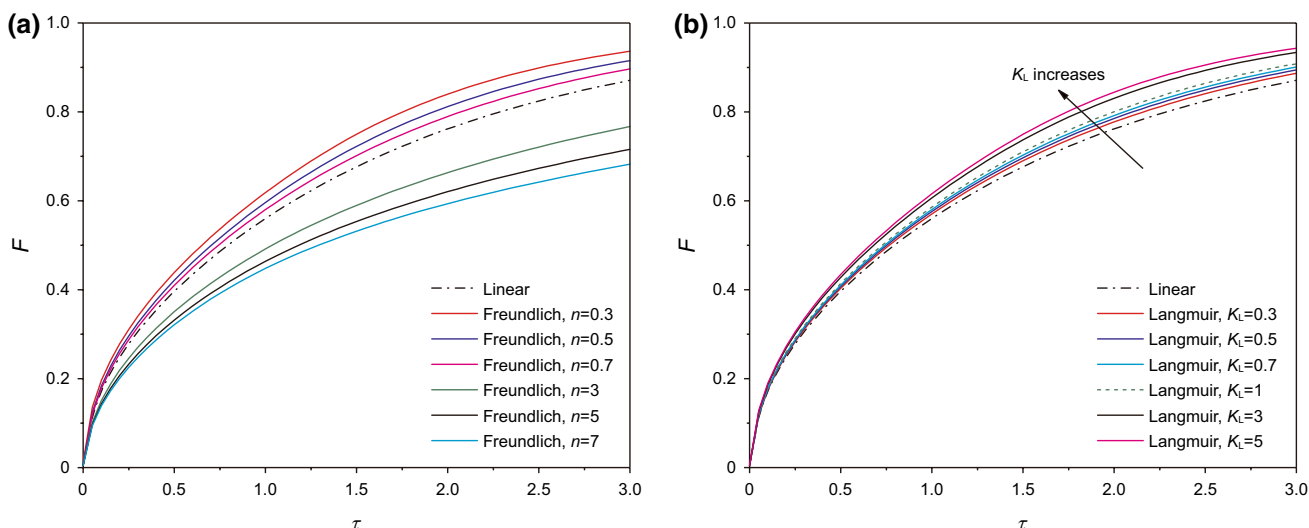


Fig. 16 The influences of adsorption isotherms on fractional uptake F with $\alpha=10$, $\beta=1$, $a/\gamma=20,000$, $K_a=1$, $K_i=1$, $\kappa=1$. **a** Freundlich isotherm with comparison to the linear isotherm. **b** Langmuir isotherm with comparison to the linear isotherm

increases with increasing κ , indicating that a large accessible area for diffusion of adsorbates from macropores to micropores contributes to intensifying the mass transfer in porous materials. But the effect of parameter κ on the fractional uptake can be negligible at a value of $\beta=10$ (high microporosity) or a value of $\beta=0.1$ (high macroporosity).

The influences of different adsorption isotherms on the fractional uptake with the same adsorption capacity (K_a , K_i) are shown in Fig. 16. For the Freundlich isotherm, the fractional uptake increases with a decreasing value of n . For $n > 1$, the fractional uptake is lower than that of the linear isotherm, while for $n < 1$, the situation is the reverse. For the Langmuir isotherm, the fractional uptake of the linear isotherm is the slowest, and the fractional uptake increases with an increasing value of K_L . It can be concluded that the nonlinear adsorption behavior can prolong or reduce the time needed to saturate the pellets with bidisperse pores in comparison with the linear isotherm. For the Freundlich isotherm $n > 1$, the time is longer than that of the linear isotherm, while for $n < 1$, the situation is the reverse. For the Langmuir isotherm, the time is shorter than that of the linear isotherm. In Silva and Rodrigues’s work (Silva and Rodrigues 1999), they also found that the time needed to saturate pellets with bidisperse pore structures is longer for the linear isotherm than that for the Langmuir isotherm.

3.3 Effects of different adsorption isotherms on the concentration distribution

The effects of the nature of the isotherms on the concentration distribution in micro- and macropores when the whole adsorption process is limited by macropore diffusion are shown in Fig. 17. For the Freundlich isotherm, the adsorbate concentrations in macro- and micropores increase with an increasing value of n . For $n > 1$, the adsorbate concentrations are greater than that of the linear isotherm, while for $n < 1$, the situation is the reverse. For the Langmuir isotherm, all the adsorbate concentrations are lower than that of the linear isotherm, and the adsorbate concentration decreases with an increasing value of K_L .

4 Conclusions

A model is proposed for transient diffusion in porous materials with bidisperse pore structures, which shows the competitive effects between micropore diffusion and macropore diffusion for the cases of the linear, Freundlich, and Langmuir adsorption equilibrium isotherms. A criterion is suggested for identifying the controlling mechanism, reflecting the competitive effects between micropore diffusion and macropore diffusion: for $\alpha < 0.001$, micropore diffusion is the controlling process; for $\alpha > 10$, macropore diffusion is the controlling process and for $0.001 < \alpha < 10$, macropore and micropore diffusions are the controlling processes. The time needed to saturate the porous materials can be shortened by increasing the diffusion rate

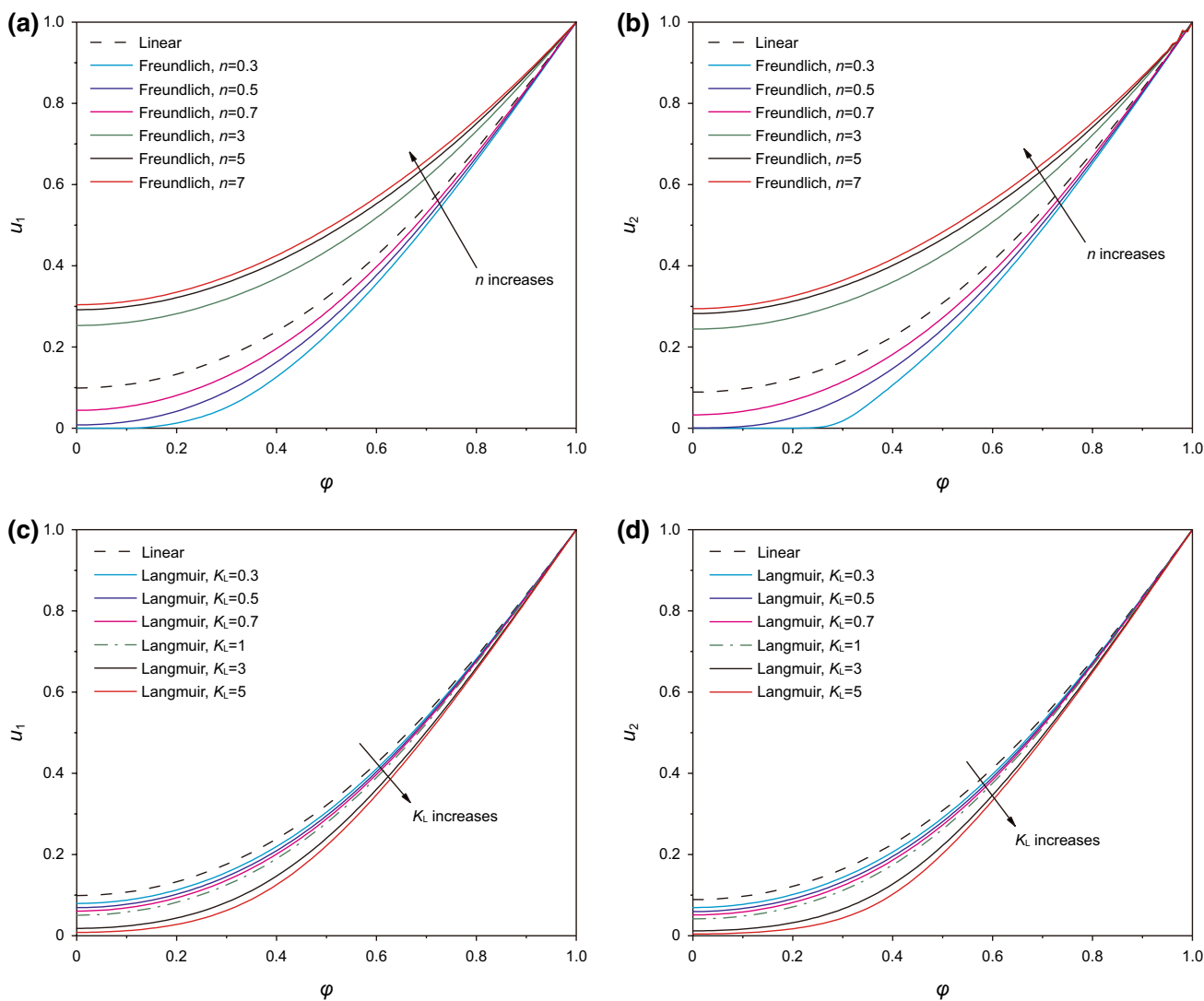


Fig. 17 The effects of different adsorption isotherms on concentration profiles versus φ at dimensionless time $\tau=1$ with $\alpha=10$, $\beta=1$, $\alpha/\gamma=20,000$, $K_a=1$, $K_i=1$, $\kappa=1$. **a** Freundlich isotherm in comparison with the linear isotherm: concentration in macropores. **b** Freundlich isotherm in comparison with the linear isotherm: concentration in micropores. **c** Langmuir isotherm in comparison with the linear isotherm: concentration in macropores. **d** Langmuir isotherm in comparison with the linear isotherm: concentration in micropores

in micropores, decreasing the ratio of micro- and macroporosity as well as the adsorption capacity K_i , and increasing the ratio κ of accessible area for diffusion from macropores to micropores.

The fractional uptake F and concentration in pores depend on the type of adsorption isotherms. For the Freundlich isotherm, when $n > 1$, the concentrations are greater than that of the linear isotherm, and the time needed to saturate the porous materials is larger than that for the linear isotherm. When $n < 1$, the cases are the reverse. For the Langmuir isotherm, the concentrations are lower than that of the linear isotherm, and the time needed to saturate the porous materials is shorter than that for the linear isotherm.

Acknowledgements The authors acknowledge the financial support by the National Natural Science Foundation of China (Grant No. 91534120) and by China National Petroleum Company under the contract number DQZX-KY-17-019.

Open Access This article is distributed under the terms of the Creative Commons Attribution 4.0 International License (<http://creativecommons.org/licenses/by/4.0/>), which permits unrestricted use, distribution, and reproduction in any medium, provided you give appropriate credit to the original author(s) and the source, provide a link to the Creative Commons license, and indicate if changes were made.

Appendix A

The area S_1 of the red shadow shown in Fig. A1 is

$$S_1 = \frac{\sqrt{3}}{4}d^2 - \frac{1}{2}\pi r^2 \tag{A1}$$

The radius R_i of a circle whose area is equivalent to S_1 is

$$R_i = \sqrt{\frac{\sqrt{3}}{4\pi}d^2 - \frac{1}{2}r^2} \tag{A2}$$

The perimeter P_1 of the red shadow is

$$P_1 = 3(d - 2r) + \pi r \tag{A3}$$

The perimeter P_2 of the circle whose area is equivalent to S_1 is

$$P_2 = 2\pi R_i = \sqrt{\sqrt{3}\pi d^2 - 2\pi^2 r^2} \tag{A4}$$

The accessible perimeter P_3 for diffusion of adsorbates from macropore to micropore is

$$P_3 = \pi r \tag{A5}$$

Therefore, the ratio κ of accessible area for diffusion of adsorbates from macropore to micropore to the total lateral area of the assumed column is

$$\kappa = \frac{P_1}{P_2} \times \frac{P_3}{P_1} = \frac{\pi r}{\sqrt{\sqrt{3}\pi d^2 - 2\pi^2 r^2}} \tag{A6}$$

Let $d = mr(m \geq 2)$, the ratio κ becomes

$$\kappa = \frac{\pi}{\sqrt{\sqrt{3}\pi m^2 - 2\pi^2}} \tag{A7}$$

For some bidisperse porous materials composed of a porous nanorod array, the accessible area for diffusion of

adsorbates from macropores to micropores equals the total lateral area of columns (nanorods). Under this situation, the ratio κ is one ($\kappa = 1$).

Appendix B

The basic equations for mass balances in macropores (Eq. B1) and micropores (Eq. B2) are:

$$\begin{aligned} \varepsilon_a \frac{\partial}{\partial x} \left[D_a \frac{\partial C_{Aa}}{\partial x} \right] + \varepsilon_i \frac{\partial}{\partial x} \left[D_i \frac{\partial \overline{C_{Ai}}}{\partial x} \right] &= \varepsilon_a \frac{\partial C_{Aa}}{\partial t} + (1 - \varepsilon_a) \rho_a S_a \frac{\partial q_{Aa}}{\partial t} \\ &+ \varepsilon_i \frac{\partial \overline{C_{Ai}}}{\partial t} + (1 - \varepsilon_a - \varepsilon_i) \rho_s S_i \frac{\partial \overline{q_{Ai}}}{\partial t} \end{aligned} \tag{B1}$$

$$\begin{aligned} D_i \frac{\varepsilon_i \kappa}{r_i} \frac{\partial}{\partial r_i} \left[r_i \frac{\partial C_{Ai}}{\partial r_i} \right] + D_i \varepsilon_i \frac{\partial}{\partial x} \left[\frac{\partial C_{Ai}}{\partial x} \right] \\ = \varepsilon_i \frac{\partial C_{Ai}}{\partial t} + (1 - \varepsilon_a - \varepsilon_i) \rho_s S_i \frac{\partial q_{Ai}}{\partial t} \end{aligned} \tag{B2}$$

where

$$\overline{C_{Ai}} = \frac{1}{\pi R_i^2} \int_0^{R_i} C_{Ai} 2\pi r_i dr_i \tag{B3}$$

$$\overline{q_{Ai}} = \frac{1}{\pi R_i^2} \int_0^{R_i} q_{Ai} 2\pi r_i dr_i \tag{B4}$$

The initial and boundary conditions are:

$$\begin{cases} C_{Aa}(0, x) = 0; & \overline{C_{Ai}}(0, x) = 0 \\ \frac{\partial C_{Aa}}{\partial x}(t, 0) = 0; & \frac{\partial \overline{C_{Ai}}}{\partial x}(t, 0) = 0 \\ C_{Aa}(t, L) = C_{A0}; & \overline{C_{Ai}}(t, L) = C_{A0} \end{cases} \tag{B5}$$

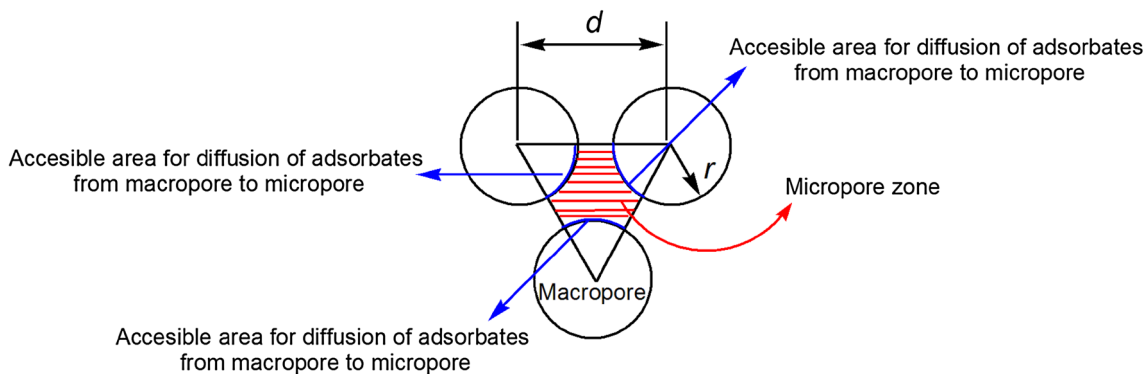


Fig. A1 The schematic diagram of a basic pore unit in bidisperse porous materials with a honeycomb structure

$$\begin{cases} C_{Ai}(0, x, r_i) = 0 \\ \frac{\partial C_{Ai}}{\partial x}(t, 0, r_i) = 0; \quad \frac{\partial C_{Ai}}{\partial r_i}(t, x, 0) = 0 \\ C_{Ai}(t, L, r_i) = C_{A0}; \quad C_{Ai}(t, x, R_i) = C_{Aa} \end{cases} \quad (B6)$$

Integration of Eq. (B2) with respect to r_i by using Eqs. (B3) and (B4) leads to:

$$\begin{aligned} \varepsilon_i \frac{\partial \overline{C_{Ai}}}{\partial t} + (1 - \varepsilon_a - \varepsilon_i) \rho_s S_i \frac{\partial \overline{q_{Ai}}}{\partial t} \\ = \frac{2\varepsilon_i \kappa D_i}{R_i} \left(\frac{\partial C_{Ai}}{\partial r_i} \right) \Big|_{r_i=R_i} + D_i \varepsilon_i \frac{\partial}{\partial x} \left[\frac{\partial \overline{C_{Ai}}}{\partial x} \right] \end{aligned} \quad (B7)$$

Evaluation of the concentration gradient at the surface $r_i=R_i$ in Eq. (B7) requires the knowledge of the concentration profiles in radial direction r_i . Assuming a parabolic concentration profile in radial direction r_i :

$$C_{Ai}(t, x, r_i) = A(t, x) + B(t, x)r_i^2 \quad (B8)$$

where $A(t, x)$ and $B(t, x)$ are the functions of time t and spatial x . The $A(t, x)$ can be determined from the boundary conditions (Eq. B6):

$$A(t, x) = C_{Ai}(t, x, R_i) - B(t, x)R_i^2 \quad (B9)$$

Substituting Eq. (B8) into Eq. (B3) leads to:

$$\overline{C_{Ai}}(t, x) = A(t, x) + \frac{1}{2}B(t, x)R_i^2 \quad (B10)$$

According to Eqs. (B9) and (B10), the $B(t, x)$ is

$$B(t, x) = \frac{2}{R_i^2} \left[C_{Ai}(t, x, R_i) - \overline{C_{Ai}}(t, x) \right] \quad (B11)$$

Therefore

$$\frac{\partial C_{Ai}}{\partial r_i} \Big|_{r_i=R_i} = \frac{4}{R_i} \left[C_{Ai}(t, x, R_i) - \overline{C_{Ai}}(t, x) \right] \quad (B12)$$

The partial differential equation of mass balance for micropores becomes:

$$\begin{aligned} \varepsilon_i \frac{\partial \overline{C_{Ai}}}{\partial t} + (1 - \varepsilon_a - \varepsilon_i) \rho_s S_i \frac{\partial \overline{q_{Ai}}}{\partial t} \\ = \frac{8\varepsilon_i \kappa D_i}{R_i^2} \left[C_{Aa} - \overline{C_{Ai}} \right] + D_i \varepsilon_i \frac{\partial}{\partial x} \left[\frac{\partial \overline{C_{Ai}}}{\partial x} \right] \end{aligned} \quad (B13)$$

According to Eq. (B13), the partial differential equation of mass balance for macropores becomes:

$$\begin{aligned} \varepsilon_a \frac{\partial C_{Aa}}{\partial t} + (1 - \varepsilon_a) \rho_a S_a \frac{\partial q_{Aa}}{\partial t} \\ = \varepsilon_a D_a \frac{\partial}{\partial x} \left[\frac{\partial C_{Aa}}{\partial x} \right] - \frac{8\varepsilon_i \kappa D_i}{R_i^2} (C_{Aa} - \overline{C_{Ai}}) \end{aligned} \quad (B14)$$

References

- Arocha MA, Jackman AP, McCoy BJ. Numerical analysis of sorption and diffusion in soil micropores, macropores, and organic matter. *Comput Chem Eng.* 1996;21(5):489–99. [https://doi.org/10.1016/S0098-1354\(96\)00288-8](https://doi.org/10.1016/S0098-1354(96)00288-8).
- Bhatia SK. Transport in bidisperse adsorbents: significance of the macroscopic adsorbate flux. *Chem Eng Sci.* 1997;52(8):1377–86. [https://doi.org/10.1016/S0009-2509\(96\)00512-X](https://doi.org/10.1016/S0009-2509(96)00512-X).
- Chu XZ, Cheng ZP, Xiang XX, et al. Separation dynamics of hydrogen isotope gas in mesoporous and microporous adsorbent beds at 77 K: SBA-15 and zeolites 5A, Y, 10X. *Int J Hydrog Eng.* 2014;39(9):4437–46. <https://doi.org/10.1016/j.ijhydene.2014.01.031>.
- Do TO, Nossou A, Springuel-Huet MA, et al. Zeolite nanoclusters coated onto the mesopore walls of SBA-15. *J Am Chem Soc.* 2004;126(44):14324–5. <https://doi.org/10.1021/ja0462124>.
- Evans PR, Yi G, Schwarzacher W. Current perpendicular to plane giant magnetoresistance of multilayered nanowires electrodeposited in anodic aluminum oxide membranes. *Appl Phys Lett.* 2000;76(4):481–3. <https://doi.org/10.1063/1.125794>.
- Glueckauf E, Coates JI. Theory of chromatography; the influence of incomplete equilibrium on the front boundary of chromatograms and on the effectiveness of separation. *J Chem Soc.* 1947;149:1315–21. <https://doi.org/10.1039/JR9470001315>.
- Lee W, Park SJ. Porous anodic aluminum oxide: anodization and templated synthesis of functional nanostructures. *Chem Rev.* 2014;114(15):7487–556. <https://doi.org/10.1021/cr500002z>.
- Lee SY, Seader JD, Tsai CH, et al. Restrictive liquid-phase diffusion and reaction in bidisperse catalysts. *Ind Eng Chem Res.* 1991;30(8):1683–93. <https://doi.org/10.1021/ie00056a002>.
- Leinekugel-Le-Cocq D, Tayakout-Fayolle M, Gorrec YL, et al. A double linear driving force approximation for non-isothermal mass transfer modeling through bi-disperse adsorbents. *Chem Eng Sci.* 2007;62(15):4040–53. <https://doi.org/10.1016/j.ces.2007.04.014>.
- Leitão A, Dias M, Rodrigues A. Effectiveness of bidisperse catalysts with convective flow in the macropores. *Chem Eng J Biochem Eng J.* 1994;55(1–2):81–6. [https://doi.org/10.1016/0923-0467\(94\)87009-8](https://doi.org/10.1016/0923-0467(94)87009-8).
- Liaw CH, Wang JSP, Greenkorn RA, et al. Kinetics of fixed-bed adsorption: a new solution. *AIChE J.* 1979;25(2):376–81. <https://doi.org/10.1002/aic.690250229>.
- Lu QY, Gao F, Komarneni S, et al. Ordered SBA-15 nanorod arrays inside a porous alumina membrane. *J Am Chem Soc.* 2004;126(28):8650–1. <https://doi.org/10.1021/ja0488378>.
- Mann R, Thomson G. Deactivation of a supported zeolite catalyst: simulation of diffusion, reaction and coke deposition in a parallel bundle. *Chem Eng Sci.* 1987;42(3):555–63. [https://doi.org/10.1016/0009-2509\(87\)80017-9](https://doi.org/10.1016/0009-2509(87)80017-9).
- Masuda H, Fukuda K. Ordered metal nanohole arrays made by a two-step replication of honeycomb structures of anodic alumina. *Science.* 1995;268(5216):1466–8. <https://doi.org/10.1126/science.268.5216.1466>.

- Muñoz B, Rámila A, Pérezpariente J, et al. MCM-41 organic modification as drug delivery rate regulator. *Chem Mater*. 2003;15(2):500–3. <https://doi.org/10.1021/cm021217q>.
- Nguyen TPB, Lee JW, Wang GS, et al. Synthesis of functionalized SBA-15 with ordered large pore size and its adsorption properties of BSA. *Microporous Mesoporous Mater*. 2008;110(2–3):560–9. <https://doi.org/10.1016/j.micromeso.2007.06.054>.
- Petersen EE. Adsorption in bidisperse-pore systems. *AIChE J*. 1991;37(5):671–8. <https://doi.org/10.1002/aic.690370505>.
- Quinta Ferreira RM, Rodrigues AE. Diffusion and catalytic zero-order reaction in a macroporous ion exchange resin. *Chem Eng Sci*. 1993;48(16):2927–50. [https://doi.org/10.1016/0009-2509\(93\)80039-S](https://doi.org/10.1016/0009-2509(93)80039-S).
- Ruckenstein E, Vaidyanathan AS, Youngquist GR. Sorption by solids with bidisperse pore structures. *Chem Eng Sci*. 1971;26(9):1305–18. [https://doi.org/10.1016/0009-2509\(71\)80051-9](https://doi.org/10.1016/0009-2509(71)80051-9).
- Selvam P, Bhatia SK, Sonwane CG. Recent advances in processing and characterization of periodic mesoporous MCM-41 silicate molecular sieves. *Ind Eng Chem Res*. 2001;40(15):3237–61. <https://doi.org/10.1021/ie0010666>.
- Shi W, Shen YQ, Ge DG, et al. Functionalized anodic aluminum oxide (AAO) membranes for affinity protein separation. *J Membr Sci*. 2008;325(2):801–8. <https://doi.org/10.1016/j.memsci.2008.09.003>.
- Silva JAC, Rodrigues AE. Analysis of ZLC technique for diffusivity measurements in bidisperse porous adsorbent pellets. *Gas Sep Purif*. 1996;10(4):207–24. [https://doi.org/10.1016/S0950-4214\(96\)00021-7](https://doi.org/10.1016/S0950-4214(96)00021-7).
- Silva VMTM, Rodrigues AE. Adsorption and diffusion in bidisperse pore structures. *Ind Eng Chem Res*. 1999;38(10):4023–31. <https://doi.org/10.1021/ie990138u>.
- Taqvi SM, Vishnoi A, Levan MD. Effect of macropore convection on mass transfer in a bidisperse adsorbent particle. *Adsorption*. 1997;3(2):127–36. <https://doi.org/10.1007/BF01650236>.
- Tartarelli R, Cioni S, Capovani M. On the second order reactions in heterogeneous catalysis. *J Catal*. 1970;37(5):671–8. [https://doi.org/10.1016/0021-9517\(70\)90179-X](https://doi.org/10.1016/0021-9517(70)90179-X).
- Turner GA. The flow-structure in packed beds: a theoretical investigation utilizing frequency response. *Chem Eng Sci*. 1958;7(3):156–65. [https://doi.org/10.1016/0009-2509\(58\)80022-6](https://doi.org/10.1016/0009-2509(58)80022-6).
- Vallet-Regi M, Rámila A, Real RPD, et al. A new property of MCM-41: drug delivery system. *Chem Mater*. 2001;13(2):308–11. <https://doi.org/10.1021/cm0011559>.
- Vinu A, Murugesan V, Hartmann M. Adsorption of lysozyme over mesoporous molecular sieves MCM-41 and SBA-15: influence of pH and aluminum incorporation. *J Phys Chem B*. 2004;108(22):7323–30. <https://doi.org/10.1021/jp037303a>.
- Wakao N, Smith JM. Diffusion in catalyst pellets. *Chem Eng Sci*. 1962;17(11):825–34. [https://doi.org/10.1016/0009-2509\(62\)87015-8](https://doi.org/10.1016/0009-2509(62)87015-8).
- Xu DS, Xu YJ, Chen DP, et al. Preparation and characterization of CdS nanowire arrays by dc electrodeposit in porous anodic aluminum oxide templates. *Chem Phys Lett*. 2000;325(4):340–4. [https://doi.org/10.1016/S0009-2614\(00\)00676-X](https://doi.org/10.1016/S0009-2614(00)00676-X).
- Zhao XS, Lu GQ. Modification of MCM-41 by surface silylation with trimethylchlorosilane and adsorption study. *J Phys Chem B*. 1998;102(9):1556–61. <https://doi.org/10.1021/jp972788m>.
- Zhao DY, Feng JL, Huo QS, et al. Triblock copolymer syntheses of mesoporous silica with periodic 50–300 angstrom pores. *Science*. 1998;279(5350):548–52.
- Zhu JZ, Shen J, Han Y. Preparation and adsorption denitrication of Nb-SBA-15 zeolite. *J Chin Ceram Soc*. 2012;40(11):1666–70 (in Chinese).